MZ-TH/12-09
TTP12-005

MSSM corrections to the top-antitop quark forward-backward asymmetry at the Tevatron

Stefan Berge[*1] **, Doreen Wackeroth**[$2]**, Martin Wiebusch**[†3]

[*] Institute for Physics (WA THEP), Johannes Gutenberg-Universität, D-55099 Mainz, Germany

[$] Department of Physics, University at Buffalo, The State University of New York, Buffalo, NY 14260-1500, U.S.A.

[†] Institute for Theoretical Particle Physics, Karlsruhe Institute of Technology (KIT), D-76128 Karlsruhe, Germany

Abstract

We study the effects of the complete supersymmetric QCD and electroweak one-loop corrections to the $t\bar{t}$ forward-backward asymmetry at the Fermilab Tevatron $p\bar{p}$ collider. We work in the complex Minimal Supersymmetric Standard Model (MSSM), only restricted by the condition of minimal flavor violation (MFV). We perform a comprehensive scan over the relevant parameter space of the complex MFV-MSSM and determine the maximal possible contributions of these MSSM loop corrections to the forward-backward asymmetry in the $t\bar{t}$ center-of-mass frame.

PACS numbers: 12.38.Bx, 12.60.Jv, 13.60.Hb, 14.65.Ha
Keywords: hadron collider physics, top quark, MSSM, forward-backward asymmetry

[1] berge@uni-mainz.de
[2] dow@ubpheno.physics.buffalo.edu
[3] wiebusch@particle.uni-karlsruhe.de

I. INTRODUCTION

Precision studies of top quark properties at the Fermilab Tevatron $p\bar{p}$ and CERN LHC pp colliders keep probing the Standard Model (SM) of electroweak (EW) and strong interactions at an increasing level of precision, and may provide a window to new physics. While the total $t\bar{t}$ cross section and $t\bar{t}$ invariant mass ($M_{t\bar{t}}$) distribution agree with SM predictions within their respective uncertainties, a measurement of the corrected (parton-level) forward-backward asymmetry in top-pair production, $A_{\rm FB}^{t\bar{t}}$, by the CDF [1–3] and D0 [4, 5] collaborations at the Tevatron

$$\begin{aligned} A_{\rm FB}^{t\bar{t}}(\text{CDF [3]}) &= 20 \pm 7_{\rm stat} \pm 2_{\rm syst}\% \\ A_{\rm FB}^{t\bar{t}}(\text{D0 [5]}) &= 19.6 \pm 6.5\% \end{aligned} \tag{1}$$

differs by about 2σ [3, 5] from the SM QCD prediction. The difference between measurement and SM QCD prediction is even more pronounced, i. e. at the 3σ level, in the region $M_{t\bar{t}} > 450$ GeV, where a measurement of $A_{\rm FB}^{t\bar{t}}$ yields [2]:

$$A_{\rm FB}^{t\bar{t}}(\text{CDF}, M_{t\bar{t}} > 450 \text{ GeV}) = 47.5 \pm 11.4\% \tag{2}$$

The forward-backward asymmetry in the $t\bar{t}$ center-of-mass (CM) frame is defined as:

$$A_{\rm FB}^{t\bar{t}} = \frac{\sigma_{t\bar{t}}(\Delta y > 0) - \sigma_{t\bar{t}}(\Delta y < 0)}{\sigma_{t\bar{t}}(\Delta y > 0) + \sigma_{t\bar{t}}(\Delta y < 0)} \tag{3}$$

where $\Delta y = y_t - y_{\bar{t}}$ denotes the difference in rapidity of the top and anti-top quark, and SM predictions including higher-order QCD and EW corrections are provided in Refs. [6–13] and Refs. [12–14], respectively. The interpretation of the observed discrepancy requires a solid understanding of the theory predictions, i. e. control of the theoretical uncertainties. Recent updated calculations and studies of theoretical uncertainties at next-to-leading order (NLO) and next-to-next-to-leading-logarithmic order (NNLL) in QCD [11, 15] and at NLO EW+QCD [12, 13] find that the discrepancy is reduced compared to NLO QCD predictions, but still persists for the measurement at large $M_{t\bar{t}}$. For instance, including the EW contributions to $\mathcal{O}(\alpha^2)$ and $\mathcal{O}(\alpha\alpha_s^2)$ to $A_{\rm FB}^{t\bar{t}}$ results in a combined NLO QCD+EW prediction of [12] (including the factorization/renormalization scale uncertainty and using MRST2004QED)

$$\begin{aligned} A_{\rm FB}^{t\bar{t}}(\text{NLO QCD+EW}) &= 8.93^{+0.79}_{-0.62}\% \\ A_{\rm FB}^{t\bar{t}}(\text{NLO QCD+EW}, M_{t\bar{t}} > 450 \text{ GeV}) &= 12.77^{+1.13}_{-0.86}\%, \end{aligned} \tag{4}$$

and when including NNLL QCD contributions $A_{\rm FB}^{t\bar{t}}$ is predicted as [11] (including the factorization/renormalization scale uncertainty and using MSTW2008):

$$\begin{aligned} A_{\rm FB}^{t\bar{t}}(\text{NLO+NNLL QCD}) &= 7.24^{+1.04}_{-0.67}\% \\ A_{\rm FB}^{t\bar{t}}(\text{NLO+NNLL QCD}, M_{t\bar{t}} > 450 \text{ GeV}) &= 11.1^{+1.7}_{-0.9}\%. \end{aligned} \tag{5}$$

However, since the first non-vanishing contribution to $A_{\rm FB}^{t\bar{t}}$ is of NLO in QCD in the $t\bar{t}$ production cross section, a conclusive answer concerning the theoretical uncertainty will only be possible once a calculation of the complete NNLO QCD corrections to $t\bar{t}$ production becomes available. Nevertheless, it is interesting to study the possibility that the observed discrepancy could be interpreted as a signal of new physics. Possible SM extensions which may give rise to large contributions to $A_{\rm FB}^{t\bar{t}}$ have been explored extensively in the literature and some recent examples can be found in Refs. [16–19]. In this paper, we consider the one-loop $\mathcal{O}(\alpha_s)$ SUSY QCD and $\mathcal{O}(\alpha)$ SUSY EW corrections to the strong partonic $t\bar{t}$ production process, $q\bar{q} \to t\bar{t}$, and study their impact on $A_{\rm FB}^{t\bar{t}}$ at the Tevatron. We work in the complex Minimal Supersymmetric SM (MSSM) [20, 21] and assume it to only be restricted by the condition of minimal flavor violation (MFV) [22, 23]. The other possible partonic process at leading-order (LO) QCD, $gg \to t\bar{t}$, is symmetric in the production rates for top quarks in the forward and backward hemisphere, and thus only enters the total cross section in the denominator of $A_{\rm FB}^{t\bar{t}}$. After a consistent perturbative expansion of $A_{\rm FB}^{t\bar{t}}$ in α_s and α, the MSSM one-loop contribution to $A_{\rm FB}^{t\bar{t}}$ calculated in this paper can then be written as follows (the dependence on α_s and α is explicitly shown):

$$A_{\rm FB}^{t\bar{t}} = \alpha_s \frac{\Delta\sigma_{t\bar{t}}^{SQCD}}{\sigma_{t\bar{t}}^{(0)}} + \alpha \frac{\Delta\sigma_{t\bar{t}}^{SEW}}{\sigma_{t\bar{t}}^{(0)}} \tag{6}$$

with $\Delta\sigma_{t\bar{t}}^{SQCD,SEW} = \delta\sigma_{t\bar{t}}^{SQCD,SEW}(\Delta y > 0) - \delta\sigma_{t\bar{t}}^{SQCD,SEW}(\Delta y < 0)$, where $\sigma_{t\bar{t}}^{(0)}$ denotes the total $t\bar{t}$ production cross section at LO QCD and $\delta\sigma_{t\bar{t}}^{SQCD,SEW}$ denote the SUSY QCD and SUSY EW one-loop contributions, respectively. The SUSY QCD and SUSY EW one-loop corrections to (unpolarized) $t\bar{t}$ production in hadronic collisions have been studied in Refs. [24–31] and Refs. [31–35], respectively. They are known to only modestly impact the total $t\bar{t}$ production cross section and invariant $t\bar{t}$ mass distribution, and thus, at the presently available precision, do not spoil the good agreement between theory and experiment for those observables, at least for sparticle masses of $\mathcal{O}(100)$ GeV (and larger) and $m_{\tilde{g}} \gtrsim 230$ GeV [30]. In this paper, we will derive general bounds on $A_{\rm FB}^{t\bar{t}}$, i. e. we work within the MFV-MSSM and scan over a large range of values for the relevant MSSM input parameters, without imposing additional constraints. In particular, these bounds do not rely, for instance, on specific SUSY breaking scenarios or an artificially reduced parameter space such as the constrained MSSM (CMSSM). As will be discussed as well, the impact of any specific assumption, e. g., mass limits derived from LHC squark and gluino searches, on the bounds on $A_{\rm FB}^{t\bar{t}}$ can then be readily deduced from these general results.

The paper is organized as follows. After presenting the calculation of the MSSM one-loop corrections that contribute to the forward-backward asymmetry in Section II, we derive analytic expressions for bounds on $A_{\rm FB}^{t\bar{t}}$ induced by SUSY QCD one-loop corrections in Section II A and discuss the structure of the SUSY EW one-loop corrections to $A_{\rm FB}^{t\bar{t}}$ in more detail in Section II B. In Section III, we present numerical results for the forward-backward

asymmetry. In Section III A, we determine general bounds on $A_{\rm FB}^{t\bar{t}}$ based on the analytic expressions derived in Section II A. In Section III B, we present a comprehensive scan over the relevant complex MFV-MSSM parameter space. We conclude in Section IV and provide explicit expressions for the relevant MSSM couplings and one-loop corrections in the appendix.

II. MSSM ONE-LOOP CONTRIBUTIONS TO $A_{\rm FB}^{t\bar{t}}$

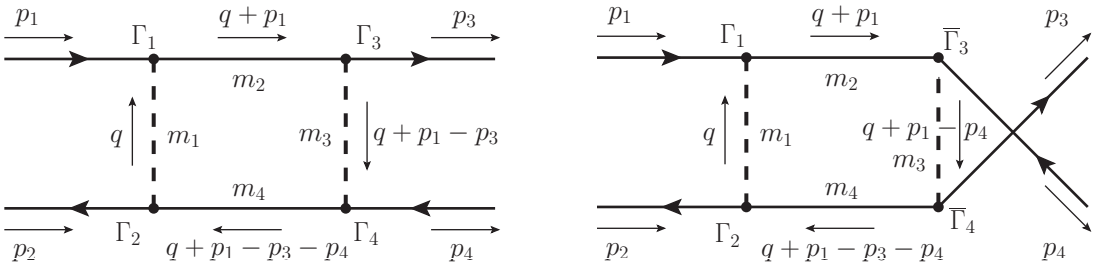

Figure 1: Momentum and mass assignments for the direct and crossed box diagrams. A possible color factor has been omitted.

In the MSSM the additional one-loop contributions to the top forward-backward asymmetry, i. e. $A_{\rm FB}^{t\bar{t}}$ of Eq. (6), originate from box diagrams involving squarks, gluinos and neutralinos inside the loops. The generic diagrams are shown in Fig. 1. The external momenta are denoted by $p_1,\ldots,p_4$ and $m_1,\ldots,m_4$ are the masses of the internal particles. The gluino-squark-quark and neutralino-squark-quark vertices are represented by Γ_n ($n=1,\ldots,4$), which we decompose, excluding a possible color factor, in the following way:

$$\Gamma_n \;=\; g_n^+ P^+ + g_n^- P^- \qquad \text{with} \qquad P^\pm = \frac{1\pm\gamma_5}{2} \quad . \tag{7}$$

The full gluino-squark-quark vertex also includes color matrices $\Gamma_n^c = T^c\cdot\Gamma_n$ with $T^c = \lambda^c/2$ and λ^c the Gell-Mann matrices. The internal masses m_n and the generic couplings $g_n^\pm$ depend on the particles that are assigned to the internal lines. Explicit expressions for $g_n^\pm$ for gluino-squark-quark and neutralino-squark-quark couplings are provided in Section V A and Section V B, respectively. For each assignment of internal particles to the direct box (Fig. 1a), we get a corresponding contribution from the crossed box (Fig. 1b) with identical values of the internal masses m_n and the coupling parameters $g_n^\pm$. The vertices $\overline{\Gamma}_n$ ($n=3,4$) are related to the Γ_n by

$$\overline{\Gamma}_n = \gamma^0\Gamma_n^\dagger\gamma^0 = g_n^{-*}P^+ + g_n^{+*}P^- .$$

The amplitudes $\mathscr{M}^{(a)}$ and $\mathscr{M}^{(b)}$ corresponding to the diagrams in Fig. 1 can be generated using the Feynman rules for fermion number violating interactions of Ref. [36] that have been implemented in FeynArts [37–39]. They are then calculated with standard trace techniques

and a Passarino-Veltman reduction [40] of the loop integrals using FORM [41]. For the direct box diagram we write the partonic differential cross section $\frac{d\hat{\sigma}^{(a)}}{d\cos\theta}$ in terms of the interference of $\mathscr{M}^{(\mathrm{a})}$ with the LO matrix element $\mathscr{M}^{(0)}$ as

$$\begin{aligned}
\frac{d\hat{\sigma}^{(a)}}{d\cos\theta} &= \frac{\beta_t}{32\pi\hat{s}}\cdot\frac{1}{4}\cdot\frac{1}{9}\sum_{\text{spins}} 2Re\left\{\mathscr{M}^{(\mathrm{a})}\mathscr{M}^{(0)*}\right\} \\
&= \frac{\beta_t}{32\pi\hat{s}}\cdot N_a \sum_{\lambda=\pm} 2Re\Big[\; g_1^{+\lambda}g_2^{-\lambda}g_3^{+\lambda}g_4^{+\lambda}D^{+-++}(\hat{s},\cos\theta) \\
&\qquad + g_1^{-\lambda}g_2^{+\lambda}g_3^{+\lambda}g_4^{+\lambda}D^{-+++}(\hat{s},\cos\theta) \\
&\qquad + g_1^{-\lambda}g_2^{+\lambda}g_3^{+\lambda}g_4^{-\lambda}D^{-++-}(\hat{s},\cos\theta) \\
&\qquad + g_1^{-\lambda}g_2^{+\lambda}g_3^{-\lambda}g_4^{+\lambda}D^{-+-+}(\hat{s},\cos\theta)\;\Big]
\end{aligned} \tag{8}$$

with $\beta_t = \sqrt{1-\frac{4m_t^2}{\hat{s}}}$ and m_t denoting the top quark mass. The sum over the index λ has to be interpreted as

$$\sum_{\lambda=\pm} g_n^{\pm\lambda} = \sum_{\lambda=+1,-1} g_n^{(\pm1)*(\lambda)} = g_n^{\pm} + g_n^{\mp}$$

with $g_n^{\pm}$ defined in Eq. (28) for SUSY QCD and in Eq. (31) for SUSY EW loop diagrams. The factors $1/4$ and $1/9$ in Eq. (8) are the spin and color average factors, respectively. The functions $D^a(\hat{s},\cos\theta)$ with

$$a \in \{+-++,-+++,-++-,-+-+\} \tag{9}$$

are given in Eq. (33). They depend on the partonic Mandelstam variables $\hat{s} = (p_1+p_2)^2 = (p_3+p_4)^2$ and by $\hat{t} = (p_1-p_3)^2 = (p_2-p_4)^2$ on the cosine of the scattering angle θ, i.e. the angle between the spatial components of p_1 and p_3. They also depend on the internal masses m_i, but these arguments are suppressed in Eq. (8) and the following discussion. Also, in Eq. (8) (and in the following discussion) it is implicitly understood that one has to sum over all possible assignments of particles to the internal lines. Note that the functions $D^a(\hat{s},\cos\theta)$ do not depend on the generic couplings $g_n^{\pm}$. The factor N_a is the color factor and contains the factor $1/9$ from the color average. The factor $1/4$ from the spin average is absorbed into the functions $D^a(\hat{s},\cos\theta)$.

The interference of the crossed box (Fig. 1b) with $\mathscr{M}^{(0)}$ can also be expressed in terms of the functions $D^a(\hat{s},\cos\theta)$. To see this, we note that the crossed box is obtained from the direct box by interchanging the momenta p_3 and p_4, reversing the fermion flow on the outgoing legs and replacing Γ_3 and Γ_4 by $\bar{\Gamma}_3$ and $\bar{\Gamma}_4$, respectively. The interchange of p_3 and p_4 is achieved by replacing $\cos\theta$ by $-\cos\theta$. When calculating the interference with the LO diagram, the appearance of fermion-number violating vertices must be handled correctly, e. g. following the rules in Ref. [36], and leads to an overall minus sign. The replacements

$\Gamma_3 \to \bar{\Gamma}_3$ and $\Gamma_4 \to \bar{\Gamma}_4$ are equivalent to $g_n^{\pm} \to g_n^{\mp *}$ ($n = 3,4$). Thus, we obtain

$$\begin{aligned}
\frac{d\hat{\sigma}^{(b)}}{d\cos\theta} &= \frac{\beta_t}{32\pi\hat{s}} \cdot \frac{1}{4} \cdot \frac{1}{9} \sum_{\text{spins}} 2Re\left\{ \mathscr{M}^{(\mathrm{b})} \mathscr{M}^{(0)*} \right\} \\
&= \frac{\beta_t}{32\pi\hat{s}} \cdot N_b \sum_{\lambda=+,-} 2Re\big[-g_1^{+\lambda} g_2^{-\lambda} g_3^{-\lambda *} g_4^{-\lambda *} D^{+-++}(\hat{s}, -\cos\theta) \\
&\qquad - g_1^{-\lambda} g_2^{+\lambda} g_3^{-\lambda *} g_4^{-\lambda *} D^{-+++}(\hat{s}, -\cos\theta) \\
&\qquad - g_1^{-\lambda} g_2^{+\lambda} g_3^{-\lambda *} g_4^{+\lambda *} D^{-++-}(\hat{s}, -\cos\theta) \\
&\qquad - g_1^{-\lambda} g_2^{+\lambda} g_3^{+\lambda *} g_4^{-\lambda *} D^{-+-+}(\hat{s}, -\cos\theta) \big]. \qquad (10)
\end{aligned}$$

with D^a of Eq. (33). Note that the interference of the crossed box with the LO matrix element $\mathscr{M}^{(0)}$ may have a different color factor than the direct box. This factor is denoted by N_b. Using Eqs. (8), (10) and $d\hat{\sigma} = d\hat{\sigma}^{(a)} + d\hat{\sigma}^{(b)}$, the corresponding partonic forward-backward asymmetry can be written in a compact form ($\hat{\sigma}_{t\bar{t}}^{(0)}$ denotes the partonic LO total $t\bar{t}$ cross section, including both the $q\bar{q}$ and gg-initiated $t\bar{t}$ production processes)

$$\begin{aligned}
\hat{A}_{FB}^{t\bar{t}}(\hat{s}) &= \frac{1}{\hat{\sigma}_{t\bar{t}}^{(0)}} \int_0^1 d\cos(\theta) \frac{d\hat{\sigma}(\hat{s}, \cos\theta)}{d\cos\theta} - \int_{-1}^0 d\cos(\theta) \frac{d\hat{\sigma}(\hat{s}, \cos\theta)}{d\cos\theta} \qquad (11) \\
&= \frac{1}{\hat{\sigma}_{t\bar{t}}^{(0)}} \int_0^1 d(\cos\theta) [\frac{d\hat{\sigma}(\hat{s}, \cos\theta)}{d\cos\theta} - \frac{d\hat{\sigma}(\hat{s}, -\cos\theta)}{d\cos\theta}] \\
&= \frac{1}{\hat{\sigma}_{t\bar{t}}^{(0)}} \int_0^1 d(\cos\theta) \sum_a Re\left\{ G_q^a \cdot \hat{A}^a(\hat{s}, \cos\theta) \right\}
\end{aligned}$$

with the index a defined in Eq. (9),

$$\hat{A}^a(\hat{s}, \cos\theta) = \frac{\beta_t}{32\pi\hat{s}} \cdot N_g \cdot [2D^a(\hat{s}, \cos\theta) - 2D^a(\hat{s}, -\cos\theta)] \qquad (12)$$

and

$$\begin{aligned}
G_q^{+-++} &= \textstyle\sum_{\lambda=+,-} \hat{g}_1^{+\lambda} \hat{g}_2^{-\lambda} (\hat{g}_3^{+\lambda} \hat{g}_4^{+\lambda} N_a + \hat{g}_3^{-\lambda *} \hat{g}_4^{-\lambda *} N_b), \\
G_q^{-+++} &= \textstyle\sum_{\lambda=+,-} \hat{g}_1^{-\lambda} \hat{g}_2^{+\lambda} (\hat{g}_3^{+\lambda} \hat{g}_4^{+\lambda} N_a + \hat{g}_3^{-\lambda *} \hat{g}_4^{-\lambda *} N_b), \\
G_q^{-++-} &= \textstyle\sum_{\lambda=+,-} \hat{g}_1^{-\lambda} \hat{g}_2^{+\lambda} (\hat{g}_3^{+\lambda} \hat{g}_4^{-\lambda} N_a + \hat{g}_3^{-\lambda *} \hat{g}_4^{+\lambda *} N_b), \\
G_q^{-+-+} &= \textstyle\sum_{\lambda=+,-} \hat{g}_1^{-\lambda} \hat{g}_2^{+\lambda} (\hat{g}_3^{-\lambda} \hat{g}_4^{+\lambda} N_a + \hat{g}_3^{+\lambda *} \hat{g}_4^{-\lambda *} N_b). \qquad (13)
\end{aligned}$$

Note that the coupling products G_q^a may, in general, depend on the initial-state quark flavor q, as indicated by the subscript. The color factors $N_{a,b}$ have been absorbed into the definition of G_q^a and all the other factors into the definition of $\hat{A}^a(\hat{s}, \cos\theta)$. An additional coupling factor N_g has been absorbed in $\hat{A}^a$ for convenience so that the coupling products G_q^a, defined in terms of $\hat{g}_n^{\pm}$ of Eqs. (29) and (32), are of $\mathscr{O}(1)$.

The hadronic forward-backward asymmetry is then defined by folding with the parton distribution functions (PDF) and by dividing by the total hadronic LO cross section $\sigma_{t\bar{t}}^{(0)}$, so that $A_{\rm FB}^{t\bar{t}}$ of Eq. (6) at the Tevatron reads

$$\begin{aligned} A_{\rm FB}^{t\bar{t}} &= \frac{1}{\sigma_{t\bar{t}}^{(0)}} \sum_q \int_0^1 dx_1 \int_0^1 dx_2 \int_0^1 d(\cos\theta) \\ &\times \Bigg[f_{q/p}(x_1) f_{\bar{q}/\bar{p}}(x_2) \sum_a Re\left\{ G_q^a \cdot \hat{A}^a(\hat{s}, \cos\theta) \right\} \theta(\hat{s} - 4m_t^2) \\ &\quad + f_{\bar{q}/p}(x_1) f_{q/\bar{p}}(x_2) \sum_a Re\left\{ G_q^a \cdot \hat{A}^a(\hat{s}, -\cos\theta) \right\} \theta(\hat{s} - 4m_t^2) \Bigg]_{\hat{s}=x_1 x_2 S} \\ &= \sum_q Re\left\{ \sum_a G_q^a A_q^a \right\} = \sum_q A_q \,, \end{aligned} \tag{14}$$

where we defined for each initial-state quark flavor q

$$\begin{aligned} A_q^a &= \frac{1}{\sigma_{t\bar{t}}^{(0)}} \int_0^1 dx_1 \int_0^1 dx_2 \int_0^1 d(\cos\theta) [f_{q/p}(x_1) f_{q/p}(x_2) - f_{\bar{q}/p}(x_1) f_{\bar{q}/p}(x_2)] \\ &\times \theta(\hat{s} - 4m_t^2) \cdot \hat{A}^a(\hat{s}, \cos\theta) \Big|_{\hat{s}=x_1 x_2 S} \end{aligned} \tag{15}$$

and

$$\begin{aligned} A_q = Re\{ &\quad G_q^{+-++} A_q^{+-++} + G_q^{-+++} A_q^{-+++} \\ &+ G_q^{-+-+} A_q^{-+-+} + G_q^{-++-} A_q^{-++-} \}. \end{aligned} \tag{16}$$

Here $\sqrt{S} = 1.96$ TeV is the Tevatron hadronic CM energy. The function $f_{q/p}(f_{\bar{q}/p})$ is the PDF of the quark(anti-quark) flavor $q(\bar{q})$ inside the proton and the functions $f_{q/\bar{p}}$ and $f_{\bar{q}/\bar{p}}$ are the corresponding PDFs for the anti-proton. In Eq. (15) we made use of the fact that at a $p\bar{p}$ collider the quark(anti-quark) distribution inside the proton coincides with the anti-quark(quark) distribution inside the anti-proton. Moreover, when the incoming momenta are interchanged (or $x_1 \leftrightarrow x_2$), it corresponds to replacing $\cos\theta$ with $-\cos\theta$. The difference in the PDFs occurs because $\hat{A}^a$ of Eq. (12) is anti-symmetric in $\cos\theta$.
In the presence of *CP* violating phases, the coupling factors G_q^a of Eq. (13) may have imaginary parts. In this case, the imaginary parts of the A_q^a may also contribute to $A_{\rm FB}^{t\bar{t}}$.
With the notations above, we have decomposed the MSSM one-loop contribution to the forward-backward asymmetry, $A_{\rm FB}^{t\bar{t}}$ of Eq. (6), into loop functions A_q^a and coupling products G_q^a. The loop functions only depend on the internal masses in the box diagrams of Fig. 1 while the dependence on the coupling constants is contained in the coupling factors G_q^a. This separation will prove very useful when we attempt to give bounds on $A_{\rm FB}^{t\bar{t}}$ in the MSSM that do not rely on specific SUSY breaking scenarios or an artificially reduced parameter space.

A. SUSY QCD One-loop Contributions

When only SUSY QCD one-loop contributions to $A_{\rm FB}^{t\bar{t}}$ are considered, the Majorana fermions in the box diagrams of Fig. 1 are all gluinos. The relevant diagrams are shown in Fig. 2. In the

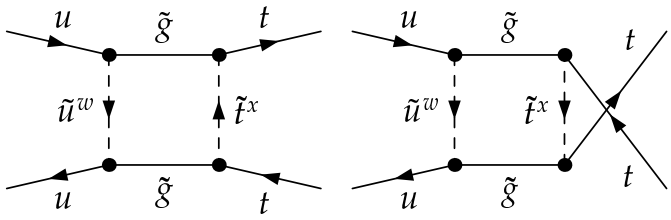

Figure 2: Feynman diagrams of the SUSY QCD one-loop contribution to the forward-backward asymmetry $A_{\rm FB}^{t\bar{t}}$.

case of SUSY QCD, Eq. (16) can be further simplified due to relations among the coupling products G_q^a and the loop functions A_q^a. The color factors in Eq. (13) and the coupling factor in Eq. (12) are now

$$N_a = \frac{7}{27} \quad , \qquad N_b = -\frac{2}{27} \quad , \qquad N_g = 4g_s^6 \, ,$$

where g_s is the strong coupling constant. The internal masses are

$$m_2 = m_4 = m_{\tilde{g}} \quad , \qquad m_1 = m_{\tilde{q}_i} \quad , \qquad m_3 = m_{\tilde{t}_j} \, ,$$

where i and j are the sfermion indices of the squark and the stop, respectively. To make the dependence on the sfermion indices explicit we use the notation

$$G_q^a \to G_{q,ij}^a \quad , \qquad A_q^a \to A_{q,ij}^a .$$

Ultimately, we must sum over the sfermion indices i and j. However, since both the internal masses and the couplings may depend on the indices i and j, we postpone that sum until the end of the discussion. Due to $m_2 = m_4$, we have the relation

$$A_{q,ij}^{+-++} = A_{q,ij}^{-+++} ,$$

as can be seen from the expressions for D^a in Section V C.
Using the unitarity of the squark mixing matrices of Eq. (30), we can simplify sums and differences of the coupling products:

$$\begin{aligned}
&G_{q,ij}^{+-++} + G_{q,ij}^{-+++} = -2(N_a+N_b) Re(U_{j,+}^{\tilde{t}} U_{j,-}^{\tilde{t}*} e^{i\phi}) \equiv (N_a+N_b) G_j^{(1)} \, , \\
&G_{q,ij}^{-++-} + G_{q,ij}^{-+-+} = (N_a+N_b) \, , \\
&G_{q,ij}^{-++-} - G_{q,ij}^{-+-+} = (N_a-N_b)(|U_{i,+}^{\tilde{q}}|^2 - |U_{i,-}^{\tilde{q}}|^2)(|U_{j,+}^{\tilde{t}}|^2 - |U_{j,-}^{\tilde{t}}|^2) \equiv (N_a-N_b) G_{ij}^{(2)}
\end{aligned}$$

Thus, we write for A_q of Eq. (16) (again we added the sfermion indices ij)

$$A_{q,ij} = Re\left\{ G_j^{(1)} A_{q,ij}^{(1)} + G_{ij}^{(2)} A_{q,ij}^{(2)} + A_{q,ij}^{(3)} \right\} \tag{17}$$

with

$$\begin{aligned} A^{(1)}_{q,ij} &= (N_a+N_b)A^{-+++}_{q,ij} \\ A^{(2)}_{q,ij} &= (N_a-N_b)\tfrac{1}{2}(A^{-++-}_{q,ij}-A^{-+-+}_{q,ij}) \\ A^{(3)}_{q,ij} &= (N_a+N_b)\tfrac{1}{2}(A^{-++-}_{q,ij}+A^{-+-+}_{q,ij}) \end{aligned} \tag{18}$$

and

$$\begin{aligned} G^{(1)}_{j} &= -2Re(U^{\tilde{t}}_{j,+}U^{\tilde{t}*}_{j,-}e^{i\phi}) \\ G^{(2)}_{q,ij} &= (|U^{\tilde{q}}_{i,+}|^2-|U^{\tilde{q}}_{i,-}|^2)(|U^{\tilde{t}}_{j,+}|^2-|U^{\tilde{t}}_{j,-}|^2)\,. \end{aligned} \tag{19}$$

Using the unitarity of the stop mixing matrix $U^{\tilde{t}}$, we find

$$G^{(1)}_1 = -G^{(1)}_2 \quad , \qquad G^{(2)}_{q,i1} = -G^{(2)}_{q,i2} \quad , \qquad G^{(2)}_{q,1j} = -G^{(2)}_{q,2j}\,. \tag{20}$$

Note that $G^{(1)}_j$ and $G^{(2)}_{q,ij}$ are always real, and one therefore only needs to consider the real part of the functions $A^q_{q,ij}$. Furthermore, the coupling product $G^{(1)}_j$ does not depend on the initial-state quark flavor q. If one assumes that the mixing matrix of the light flavor squarks $\tilde{q}$ is diagonal, as in almost all of the considered parameter space, $G^{(2)}_{q,ij}$ reduces to

$$G^{(2)}_{q,ij} = (-1)^i\cdot(|U^{\tilde{t}}_{j,+}|^2-|U^{\tilde{t}}_{j,-}|^2) \equiv G^{(2)}_{ij} \tag{21}$$

and does not depend on the initial-state quark flavor q either. We can thus perform the sum over i, j and q and obtain

$$A^{t\bar{t}}_{\mathrm{FB,SQCD}} = G^{(1)}_1 A^{(1)} + G^{(2)}_{11} A^{(2)} + A^{(3)} \tag{22}$$

with

$$\begin{aligned} A^{(1)} &= \sum_{q=u,d,s,c} Re[A^{(1)}_{q,11}-A^{(1)}_{q,12}+A^{(1)}_{q,21}-A^{(1)}_{q,22}]\,, \\ A^{(2)} &= \sum_{q=u,d,s,c} Re[A^{(2)}_{q,11}-A^{(2)}_{q,12}-A^{(2)}_{q,21}+A^{(2)}_{q,22}]\,, \\ A^{(3)} &= \sum_{q=u,d,s,c} Re[A^{(3)}_{q,11}+A^{(3)}_{q,12}+A^{(3)}_{q,21}+A^{(3)}_{q,22}]\,. \end{aligned} \tag{23}$$

Note that $A^{(1)}$ vanishes for degenerate stop masses and $A^{(2)}$ vanishes if the stop or squark masses are degenerate. Upper and lower limits on the SUSY QCD one-loop contribution to $A^{t\bar{t}}_{\mathrm{FB}}$ can now be obtained for given values of the squark masses by exploiting the fact that the limits of $G^{(1)}_1$ and $G^{(2)}_{11}$ are

$$-1 \le G^{(1)}_1 \le 1\,,\ -1 \le G^{(2)}_{11} \le 1$$

and thus

$$A^{(3)} - |A^{(1)}| - |A^{(2)}| \le A^{t\bar{t}}_{\mathrm{FB,SQCD}} \le A^{(3)} + |A^{(1)}| + |A^{(2)}|\,. \tag{24}$$

B. SUSY EW One-loop Contributions

The SUSY EW one-loop contributions to the forward-backward asymmetry $A_{\rm FB}^{t\bar{t}}$ of Eq. (14) consists of four diagrams, two direct boxes and two crossed boxes, shown in Fig. 3. We again

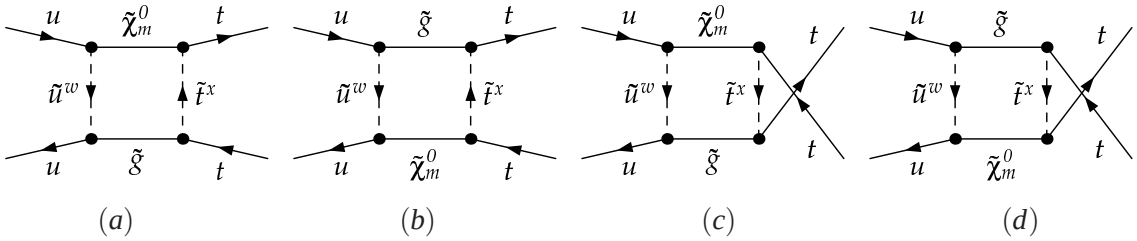

Figure 3: Feynman diagrams of the SUSY EW one-loop contribution to the forward-backward asymmetry $A_{\rm FB}^{t\bar{t}}$.

start with the generic expression for $A_{\rm FB}^{t\bar{t}}$ in terms of loop functions and coupling products as given in Eq. (16). The color factors in Eq. (13) and the coupling factor in Eq. (12) are now

$$N_a = N_b = \frac{2}{9} \quad , \qquad N_g = 4g_s^4 e^2 \, ,$$

where e is the electromagnetic coupling. The internal masses are

$$\begin{aligned} & m_1 \;=\; m_{\tilde{q}_i} \,,\; m_3 = m_{\tilde{t}_j} \,, \\ \text{Fig.}\,3(a,c)\text{:} \quad & m_2 \;=\; m_{\tilde{\chi}_k} \,,\; m_4 \;=\; m_{\tilde{g}} \qquad \text{or} \qquad \text{Fig.}\,3(b,d)\text{:}\; m_2 \;=\; m_{\tilde{g}} \,,\; m_4 \;=\; m_{\tilde{\chi}_k} \end{aligned}$$

where i and j are the sfermion indices of the squark and the stop, respectively, and k is the neutralino index. To make the dependence on the sfermion and neutralino indices explicit, we use the notation

$$G_q^a \to G_{q,kij}^a \quad , \qquad A_q^a \to A_{q,kij}^a \, .$$

Ultimately, we must sum over the indices i, j and k. This are 16 combinations for each diagram. By examining the amplitudes for the individual diagrams one notices that the diagrams (a) and (c) in Fig. 3 are the complex conjugates of the diagrams (b) and (d), respectively. Thus, the $A_{q,ij}^a$ are real and only the real parts of the coupling functions G_q^a of Eq. (13) contribute. The contribution of the SUSY EW one-loop corrections to $A_{\rm FB}^{t\bar{t}}$ of Eq. (16) then reads

$$\begin{aligned} A_{FB,SEW}^{t\bar{t}} \;&=\; \sum_q A_q \\ &=\; \sum_q \sum_{k=1}^{4} \sum_{i,j=1}^{2} \Big[\quad Re\left\{ G_{q,kij}^{+-++} \right\} A_{q,kij}^{+-++} + Re\left\{ G_{q,kij}^{-+++} \right\} A_{q,kij}^{-+++} \qquad (25) \\ &\qquad\qquad + Re\left\{ G_{q,kij}^{-++-} \right\} A_{q,kij}^{-++-} + Re\left\{ G_{q,kij}^{-+-+} \right\} A_{q,kij}^{-+-+} \Big] \qquad (26) \end{aligned}$$

In case of SUSY EW one-loop corrections, it is quite complicated to analytically derive bounds on the coupling factors $G^a_{q,kij}$ because of the complicated structure of the neutralino-squark-quark couplings (see Eq. (32)). It is even harder then to find reasonable bounds on $A^{t\bar{t}}_{FB,SEW}$ as we did in the SUSY QCD case. The box diagrams have 16 different squark und neutralino mass combinations where always some cancellation occurs due to the unitarity of the mixing matrices. Therefore, we performed a MSSM parameter scan to extract bounds on $A^{t\bar{t}}_{FB,SEW}$ as described in Section III B.

III. NUMERICAL RESULTS

For the numerical evaluation of the forward-backward asymmetry $A^{t\bar{t}}_{\rm FB}$ of Eq. (14), we use the LO PDF set CTEQ6L1 [42] with the renormalization (μ_R) and factorization (μ_F) scales chosen to be equal to the top quark mass, $\mu_R = \mu_F = m_t$. The SM input parameters are $m_t = 173.2$ GeV, $\alpha = 1/137.036$, $M_W = 80.36$ GeV, $M_Z = 91.187$ GeV, and $\cos\theta_W = M_W/M_Z$. We assume one-loop running of the strong coupling constant with $\alpha_s(M_Z) = 0.130$, so that $\alpha_s(m_t) = 0.118$, which is consistent with our choice of PDFs. To evaluate the coefficients of the tensor integrals $D_{i,ij}$ of Eq. (33), the LoopTools library [43] has been used.
The study of the dependence of $A^{t\bar{t}}_{\rm FB}$ on the MSSM input parameters is simplified by the fact that it is not sensitive to all parameters of the complex MFV-MSSM. First of all, the forward-backward asymmetry can only come from diagrams with up or down quarks in the initial state. For strange, charm and bottom quarks, the PDFs are the same as those of the corresponding anti-quarks so that the difference of PDFs in Eq. (15) is zero. In the MFV-MSSM $A^{t\bar{t}}_{\rm FB}$ is therefore insensitive to parameters that only affect the masses and couplings of strange, charm and bottom-squarks. Furthermore, the trilinear couplings of up and down-squarks only enter through the squark mass matrices, where they are suppressed by the small up and down-quark Yukawa couplings. Thus, only the following set of MSSM input parameters are relevant to our study:

- $\tan\beta$
- μ
- the pseudoscalar Higgs mass m_A
- the gaugino masses M_1, M_2 and M_3
- the top-squark trilinear coupling A_t
- the soft masses $m_{\tilde{q}_{L1}}$ and $m_{\tilde{q}_{L3}}$ of the left-handed first and third generation squarks
- the soft masses $m_{\tilde{u}_R}$, $m_{\tilde{d}_R}$ and $m_{\tilde{t}_R}$ of the right-handed up, down and top squarks

Of these parameters, μ, M_1, M_2, M_3 and A_t can be complex, but one of these phases can be rotated away. We rotate the phase of M_2 away and study the dependence on the remaining complex phases and the absolute values of the above MSSM parameters independently.
These input parameters are constrained by direct SUSY searches at LEP, Tevatron and LHC, and indirectly by low-energy precision observables. A review of results from the search for signals of low-energy SUSY at LEP and the Tevatron as well as in precision observables can be found, e. g., in Ref. [44]. Most recently stringent exclusion limits on squark and gluino masses within the CMSSM and Simplified Models have been obtained at the LHC by the CMS [45–47] and ATLAS [48–51] collaborations. In Section III B we provide general upper and lower bounds on $A_{\rm FB}^{t\bar{t}}$ within the complex MFV-MSSM by performing a comprehensive scan over a wide range of values for these input parameters without any additional assumptions. In particular, these general bounds do not rely, for instance, on specific SUSY breaking scenarios or an artificially reduced parameter space such as the CMSSM. The results are presented in such a way that the effect of a change in the sparticle mass limits on the upper and lower bounds on $A_{\rm FB}^{t\bar{t}}$ can be estimated. In Section III B this is done for the current LHC squark and gluino mass limits.
In the next sections we first discuss the main characteristics of the MSSM one-loop corrections to $A_{\rm FB}^{t\bar{t}}$ and then present results of a comprehensive parameter scan.

A. SUSY QCD and SUSY EW Contributions to the Loop Functions

The main characteristics of the MSSM one-loop corrections to, and of bounds on, $A_{\rm FB}^{t\bar{t}}$ can be determined by studying the SUSY QCD loop functions $A_{q,ij}^{(k)}$ of Eq. (18) and SUSY EW loop functions $A_{q,ijk}^{a}$ of Eq. (26). Here we will only present results for the contribution of the $u\bar{u}$-initiated $t\bar{t}$ production process, since the $d\bar{d}$ production channel is much smaller due to the smaller PDF (about a factor of eight smaller as discussed in Section III B).
In case of SUSY QCD contributions we showed in Section II A that bounds on $A_{FB,SQCD}^{t\bar{t}}$ of Eq. (18) can be derived in terms of the normalized hadronic loop functions $A_{q,ij}^{(k)}, k = 1,2,3$, where q denotes the initial-state quark flavor, i the squark index $i = 1,2$ with flavor q, and $j = 1,2$ refers to the top squark index. These loop functions only depend on three general mass parameters, $m_1 = m_{\tilde{q}_i}$, $m_2 = m_{\tilde{g}}$, and $m_3 = m_{\tilde{t}_j}$, as indicated in Figs. 1,2. For the special case of initial-state up-type quarks and mass degeneracy, $m_1 = m_2 = m_3 = M$, we show numerical results for the functions $A_{u,ij}^{(k)}$ ($k = 1,2,3$) in Figs. 4(a) and 5. As can be seen in Fig. 4(a), the largest single contribution to the loop functions comes from $A_{u,ij}^{(2)}$. This feature persists when the masses are varied independently. $A_{u,ij}^{(2)}$ reaches up to $+0.9\%$ for $M \approx 100$ GeV and -0.5% for $M \approx 200$ GeV. The other two loop functions can reach roughly $+0.4\%$ for $M \approx 100$ GeV and only tiny negative values. For masses $M \geq 400$ GeV all contributions are very small. The first peak in Figs. 4(a) and (b) at $M = 86.6$ GeV is due to a normal threshold [52] when the condition $p_3^2 = (m_2 + m_3)^2$ or $p_4^2 = (m_3 + m_4)^2$ is fulfilled,

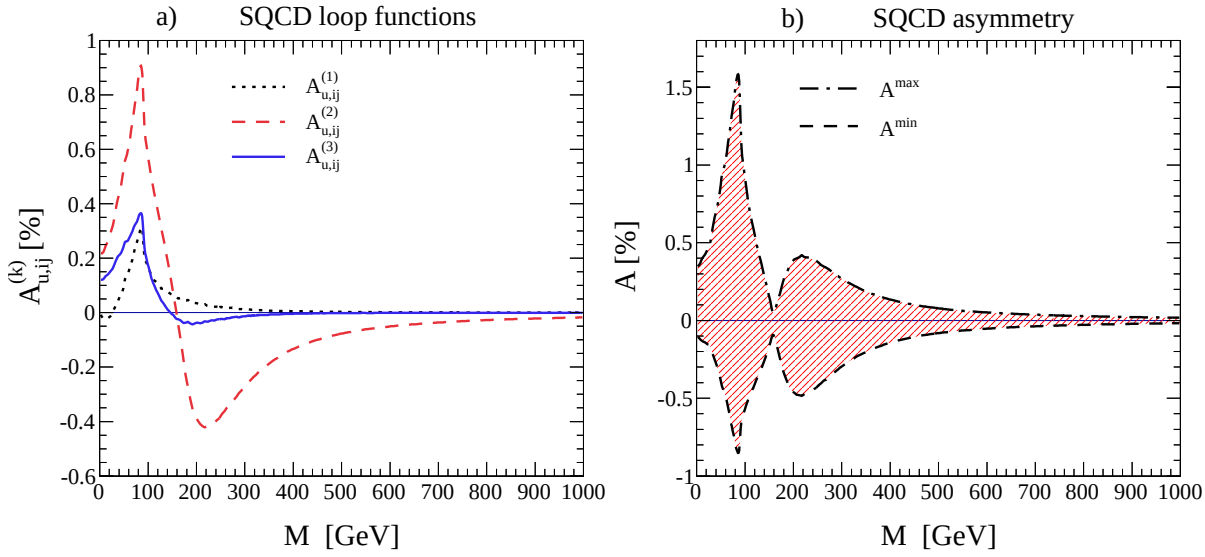

Figure 4: (a) SUSY QCD normalized hadronic loop functions $A^{(k)}_{u,ij}$ with $k = 1,2,3$ as defined in Eq. (18) and (b) bounds $A_{min,max}$ on $A^{t\bar{t}}_{\mathrm{FB,SQCD}}$ of Eq. (27) for initial-state up-quarks. Shown is the dependence on a common mass M. The bounds are obtained assuming large up-squark and top-squark mass splittings. No kinematic cuts have been applied.

which here is the case when $M = m_t/2$. A resonance in the partonic $t\bar{t}$ cross section occurs when the gluino pair in the box diagrams can become on-shell, thus $m_{\tilde{g}} > m_t$. This resonance manifests itself as dips in the hadronic functions $A^{(k)}_{u,ij}$ at $M \approx 200$ GeV. When the resonance occurs inside the numerically important $t\bar{t}$ invariant mass region of $\sqrt{\hat{s}} = 350$ to 500 GeV, it leads to a correspondingly large negative asymmetry. For larger SUSY particle masses M, the resonance region is shifted to larger values of $\sqrt{\hat{s}}$ and therefore outside the dominant region of the $t\bar{t}$ cross section. From these results an estimate of the bounds $A_{min,max}$ on $A^{t\bar{t}}_{\mathrm{FB,SQCD}}$ can be obtained using Eqs. (23) and (24). As noted earlier, $A^{(1)}$ vanishes for degenerate stop masses and $A^{(2)}$ vanishes if the stop or squark masses are degenerate. In general, we found that the SUSY QCD one-loop corrections to the forward-backward asymmetry increase if the up-squark mass splitting or, in particular, the top-squark mass splitting are increased. Thus, the largest asymmetry is obtained if $\tilde{u}_2$ and $\tilde{t}_2$ are decoupled, which results in vanishing functions $A^{(k)}_{u,12}$, $A^{(k)}_{u,21}$, and $A^{(k)}_{22}$. In this scenario the bounds of Eq. (24) read:

$$\begin{aligned} A_{min} &= A^{(3)}_{u,11} - |A^{(1)}_{u,11}| - |A^{(2)}_{u,11}| \\ A_{max} &= A^{(3)}_{u,11} + |A^{(1)}_{u,11}| + |A^{(2)}_{u,11}| \,. \end{aligned} \tag{27}$$

Figure 4(b) shows the dependence of these bounds $A_{min,max}$ on $M = m_{\tilde{t}_1} = m_{\tilde{u}_1} = m_{\tilde{g}}$. The total asymmetry can reach values from -0.9% up to $+1.6\%$ for this configuration when no kinematic cuts have been applied.

Figures. 5(a) and (b) show the loop functions $A^{(k)}_{u,ij}$ in dependence of a cut on $M_{t\bar{t}}$, $M^{min}_{t\bar{t}}$, and on $|\Delta y|$, Δy_{min}, respectively. From $M^{min}_{t\bar{t}} = 350$ GeV to $M^{min}_{t\bar{t}} = 600$ GeV, the functions $A^{(2)}_{u,ij}$

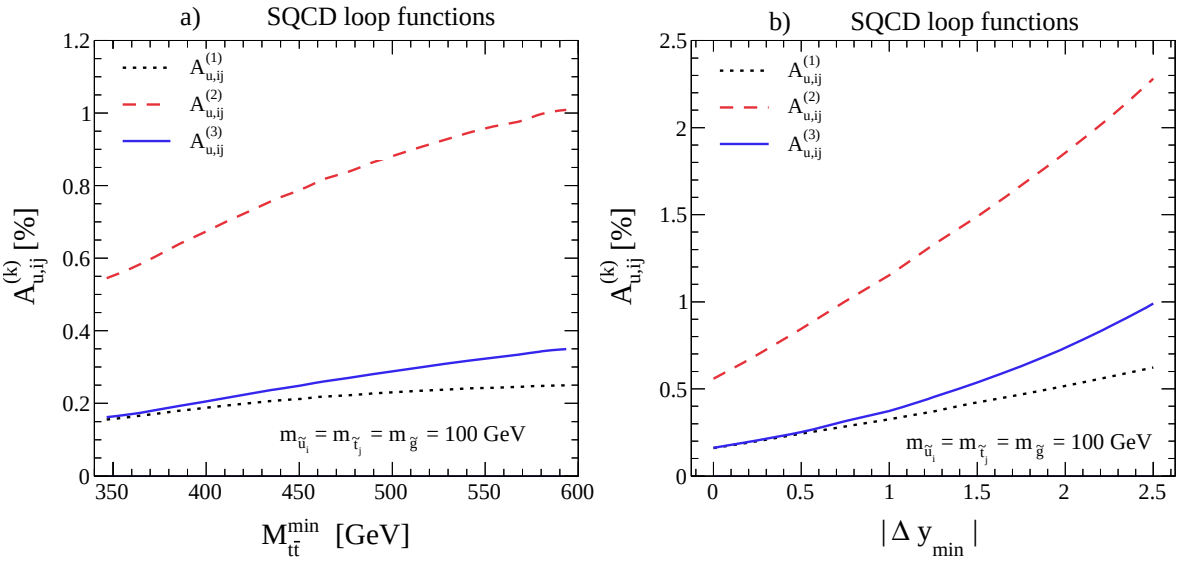

Figure 5: SUSY QCD normalized hadronic loop functions $A^{(k)}_{u,ij}$ with $k = 1,2,3$ for initial-state up-quarks as defined in Eq. (18), assuming all particles in the loop have a common mass $M = 100$ GeV. Shown is the dependence on the cut on (a) the invariant $t\bar{t}$ mass $M_{t\bar{t}}$, $M_{t\bar{t}} > M^{min}_{t\bar{t}}$, and on (b) the rapidity difference $|\Delta y| = |y_t - y_{\bar{t}}|$, $|\Delta y| > \Delta y_{min}$.

and $A^{(3)}_{u,ij}$ roughly double in size while $A^{(1)}_{u,ij}$ increases by about 50%. If one increases $M^{min}_{t\bar{t}}$ from 350 GeV to 450 GeV, the loop functions increase by a factor of 1.35 for $A^{(1)}_{u,ij}$, 1.43 for $A^{(1)}_{u,ij}$ and 1.52 for $A^{(3)}_{u,ij}$. Thus, the bounds on the forward-backward asymmetry for the SUSY QCD contributions will roughly change by a factor of 1.4 if one applies a $M^{min}_{t\bar{t}} = 450$ GeV cut compared to the case without such a cut. Applying a cut on $|\Delta y|$, as shown in Fig. 5(b), also increases the loop functions $A^{(k=1,2,3)}_{u,ij}$. For instance, when changing Δy_{min} from zero to one, $A^{(1,2)}_{u,ij}$ increase by a factor of 2.00 and $A^{(3)}_{u,ij}$ by a factor of 2.25.

We now investigate the loop functions of the SUSY EW one-loop contributions to the forward-backward asymmetry as described by $A^{t\bar{t}}_{FB,SEW}$ of Eq. (26). In this case, one has four different masses in the loop and four different loop functions $A^{a}_{u,ijk}$ with $a \in \{+-++,-++-,-+-+\}$. If one plots these loop functions in dependence of a common SUSY mass M, one can produce a similar plot as in Fig. 4, just rescaled by the smaller coupling factor and different color factors. To illustrate the effect of the neutralino mass we therefore show in Fig. 6 the loop functions for the SUSY EW one-loop contributions as defined in Eq. (25) in dependence of the neutralino mass, when assuming a common mass for the other sparticles in the loop: $M = m_{\tilde{g}} = m_{\tilde{t}_j} = m_{\tilde{u}_i} = 100$ GeV. The loop functions $A^{-++-}_{u,ijk}$ and $A^{-+-+}_{u,ijk}$ give the largest contributions. They can amount to about $\pm 0.04\%$ and only slowly decrease with increasing neutralino mass, e. g., they are still about $\pm 0.02\%$ for relatively large neutralino masses $m_{\tilde{\chi}^0_k} \approx 700$ GeV.

As stated in Section II B, it is difficult to obtain an analytic expression for bounds on $A^{t\bar{t}}_{FB,SEW}$ like it was done in case of SUSY QCD-induced asymmetries. We refer therefore to the next

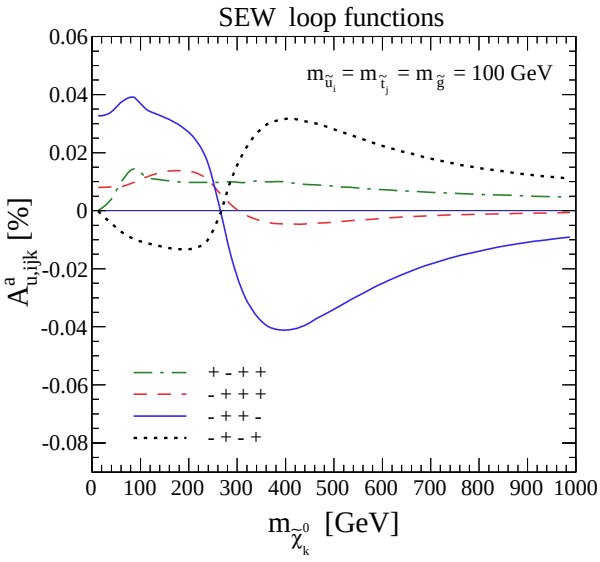

Figure 6: SUSY EW normalized hadronic loop functions $A^a_{u,ijk}$ with $a \in \{+-++,-+++,-++-,-+-+\}$ for initial-state up-quarks as defined in Eq. (25) in the case where the up-squark, top squark and the gluino have a common mass $M = m_{\tilde{g}} = m_{\tilde{t}_j} = m_{\tilde{u}_i} = 100$ GeV. Shown is the dependence on the neutralino mass $m_{\chi^0_k}$. No kinematic cuts have been applied.

section where we perform a comprehensive scan over the relevant MFV-MSSM parameter space to determine the largest possible value of $A^{t\bar{t}}_{\mathrm{FB}}$ induced by both SUSY QCD and SUSY EW one-loop corrections.

B. Bounds on $A^{t\bar{t}}_{\mathrm{FB}}$ from a MSSM parameter scan

In phenomenological studies of the MSSM the large number of parameters is a common problem. Even if all parameters of the soft MSSM Lagrangian are assumed to be real and all flavor structures are assumed to be proportional to the SM Yukawa matrices (minimal flavor violation) we are left with 30 independent parameters [53]. Numerical discussions of observables within the MSSM are therefore often limited to constrained scenarios, where certain assumptions about the SUSY breaking mechanism are imposed, or even to individual benchmark points which are deemed "representative" in some sense. Here we describe in detail how we performed a comprehensive scan over the relevant parameter space of the complex MFV-MSSM to determine bounds on $A^{t\bar{t}}_{\mathrm{FB}}$.

In the case of $A^{t\bar{t}}_{\mathrm{FB}}$, we are actually able to scan the full relevant parameter space of the complex MFV-MSSM. This is made possible by the separation of $A^{t\bar{t}}_{\mathrm{FB}}$ into loop functions A^a_q and products of coupling parameters G^a_q, which is described in Section II. Calculating the loop functions of Eq. (15) requires a numerical phase space integration and is therefore rather time-consuming. However, the A^a_q are relatively smooth functions of only four variables (namely, the internal masses $m_1, \ldots, m_4$). The loop functions may therefore be calculated

on a four-dimensional "mass-grid" and linear interpolation can be used to obtain A_q^a for other mass values within the grid range. The remaining computational cost of calculating masses and coupling constants for a given set of MSSM parameters and interpolating the loop functions is extremely small, so that sampling up to one billion (!) MSSM parameter points is perfectly doable on a single core computer.

Let us briefly discuss the details of the grid interpolation and the parameter scan. Grid data for the loop functions were generated for masses between 0 and 2 TeV. For masses below 500 GeV the grid spacing was 20 GeV. If one of the masses exceeds 500 GeV the grid spacing was increased to 50 GeV in that direction. If a mass exceeds 1 TeV the grid spacing was increased again to 100 GeV. At each grid point the integrals in Eq. (15) were calculated with the VEGAS algorithm. Specifically, we use the OmniComp-Dvegas package [54], which facilitates parallelized adaptive Monte Carlo integration and was developed in the context of [55, 56]. A lower cut of 450 GeV on the $t\bar{t}$ invariant mass was applied throughout. Thus, all the results in this section are for the 'large $m_{t\bar{t}}$' bin. Separate integrations of A_q^a were done for each value of the superscript a (three for the SUSY QCD contributions and four for the SUSY EW contributions), but the values for different quark flavors q were determined with the same simulation. Adaptation was driven by the u-quark flavor, which always produces the largest value. The relative accuracy of the numerical integration was required to be below 1%.

The multivariate linear interpolation was done by successively using one-dimensional linear interpolation in each of the variables. If, during the parameter scan, a certain mass exceeds 2 TeV the loop functions where it enters are assumed to be zero. In doing this, we neglect loop functions of the order of one permille. The discrepancies between the exact and the interpolated values of the loop functions are of the same order.

As discussed earlier, the parameter scan is simplified by the fact that $A_{\rm FB}^{t\bar{t}}$ is not sensitive to all parameters of the complex MFV-MSSM. Our choice of relevant MSSM input parameters is listed in the beginning of Section III. The value of $\tan\beta$ was varied between 1 and 50 and all parameters with mass dimension one were varied between 0 and 3 TeV. The complex phases of μ, M_1, M_3 and A_t were varied between 0 and 2π.

For the actual scan we used an adaptive method along the lines of Ref. [57]. The basic idea is the following: Instead of sampling all parameters with a uniform (or otherwise fixed) random distribution, one defines an importance function which quantifies the importance of a given set of parameters. Since we are interested in MSSM parameter points with large effects in $A_{\rm FB}^{t\bar{t}}$ we used $|A_{\rm FB}^{t\bar{t}}|$ as importance function. We then used VEGAS to compute the integral of the importance function over all the scan parameters. Adaptation guarantees that the "important" regions of the parameter space are sampled with a higher density. The OmniComp-Dvegas package [54] was used for the parameter scan too. A total of $8 \cdot 10^9$ parameter points were sampled. Adaptation was done with 22 iterations.

With the data from our scan, we can now show results for upper and lower bounds on $A_{\rm FB}^{t\bar{t}}$

as a function of any relevant MSSM input parameter. To do this, we simply bin the sample points with respect to that input parameter and determine the maximal and minimal value of $A_{\rm FB}^{t\bar{t}}$ in each bin.
Fig. 7 shows the upper and lower bounds on $A_{\rm FB}^{t\bar{t}}$ as a function of the gluino mass. Shown separately are the contributions from the $u\bar{u}$ and $d\bar{d}$-initiated $t\bar{t}$ production channels as well as from SUSY QCD and SUSY EW one-loop corrections, assuming $M_{t\bar{t}} > 450$ GeV.

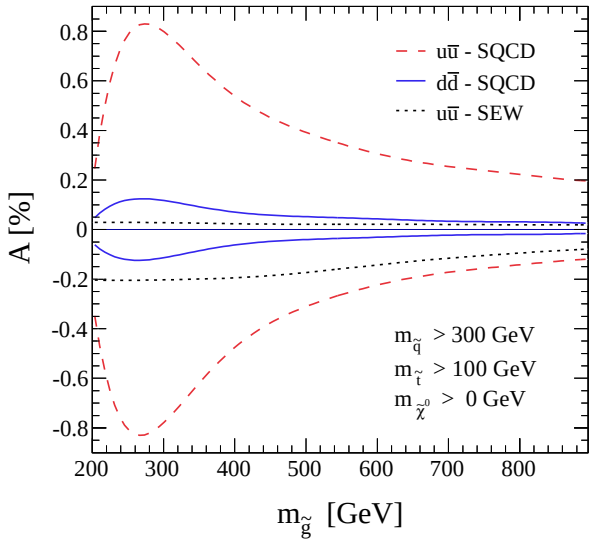

Figure 7: The gluino mass dependence of the lower and upper bound on $A_{\rm FB}^{t\bar{t}}$, $|A_{\rm FB}^{t\bar{t}}| \leq A$, due to SUSY QCD and SUSY EW one-loop contributions, with $M_{t\bar{t}} > 450$ GeV. Separately shown are the bounds when only including the $u\bar{u}$ and $d\bar{d}$-initiated $t\bar{t}$ production channels.

The bounds shown in Fig. 7 have been obtained by assuming a lower limit on the top squark masses of $m_{\tilde{t}_{1,2}} > 100$ GeV and a mass limit for the other squark flavor masses of $m_{\tilde{q}_{1,2}} > 300$ GeV. For the neutralinos no mass limit was imposed. As discussed earlier, the $u\bar{u}$-channel generates the largest contribution to $A_{\rm FB}^{t\bar{t}}$ due to the large PDF and is roughly a factor of eight larger than contribution from the $d\bar{d}$-channel. The SUSY QCD bounds peak around $m_{\tilde{g}} \approx 270$ GeV, when the contribution of the resonant gluino pair in the box diagrams coincides with the maximum of the LO $M_{t\bar{t}}$ distribution. The absolute values of the upper and lower bounds are practically identical because for the applied squark limits the SUSY QCD loop function $A_{q,ij}^{(2)}$ is dominant (see Fig. 4), so that the SUSY QCD bound of Eq. (24) is well approximated by $-|A^{(2)}| \leq A_{\rm FB,SQCD}^{t\bar{t}} \leq |A^{(2)}|$.
As shown in Fig. 7, the bounds on the SUSY EW one-loop corrections to $A_{\rm FB}^{t\bar{t}}$ are much smaller than the SUSY QCD one-loop corrections, since they are suppressed by the smaller electroweak coupling. Furthermore, the bounds are not as symmetric as in the SUSY QCD case. In general we found the absolute value of the lower bound to be larger than the upper bound. The SUSY EW one-loop corrections to the $d\bar{d}$-channel are not shown in Fig. 7 as they are basically zero, being suppressed by both the d-quark PDF and the electroweak

coupling. Again, larger SUSY EW loop-induced asymmetries can be obtained when relaxing the constraints on the MSSM parameters. For instance, for sparticle masses below 50 GeV one can obtain $A_{FB,SEW}^{t\bar{t}} = -0.4\%$.

Combining the SUSY QCD and SUSY EW one-loop contributions as well as taking into account all $q\bar{q}$-initiated $t\bar{t}$ production channels, the lower and upper bounds on $A_{\rm FB}^{t\bar{t}}$ in the complex MFV-MSSM, A_{min} and A_{max}, are shown in Figs. 8 and 9. In Fig. 8 we

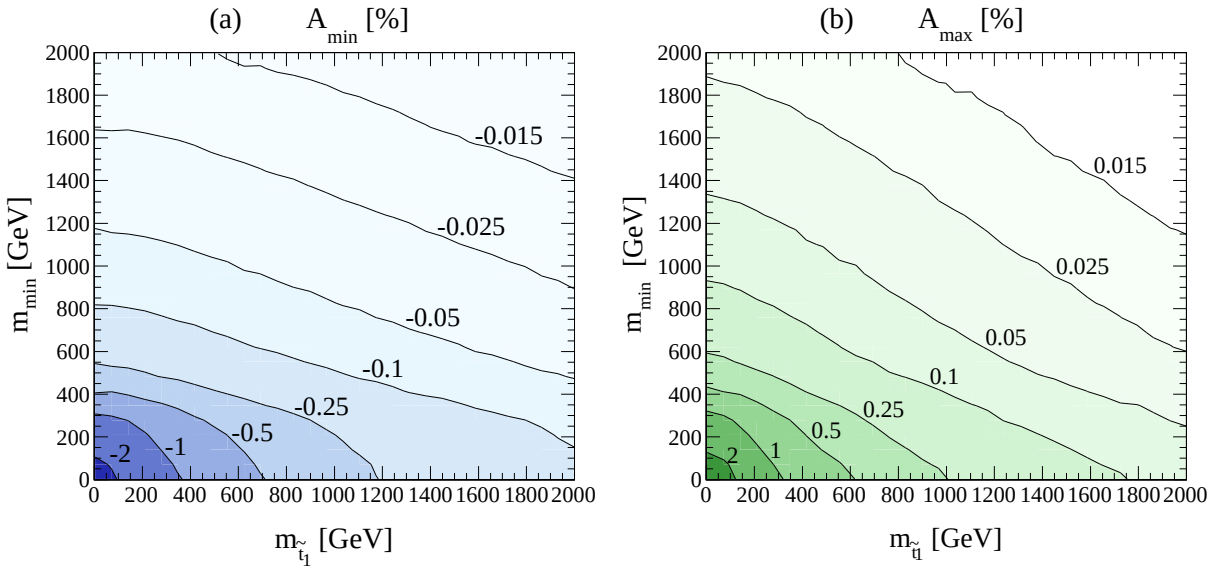

Figure 8: Bounds on the MSSM one-loop contributions to $A_{\rm FB}^{t\bar{t}}$ with $M_{t\bar{t}} > 450$ GeV: (a) Lower and (b) upper bounds on $A_{\rm FB}^{t\bar{t}}$ (in percent) as functions of the lighter top squark mass $m_{\tilde{t}_1}$ and m_{min}, which is the lightest other SUSY particle in the loops except for $m_{\tilde{t}_2}$, i. e. $m_{min} = \text{Min}\{\text{m}_{\tilde{\text{g}}}, \text{m}_{\tilde{\chi}_{1,2,3,4}}, \text{m}_{\tilde{\text{u}}_{1,2}}, \text{m}_{\tilde{\text{d}}_{1,2}}\}$.

show the dependence of the bounds $A_{min,max}$ on the lighter stop quark mass $m_{\tilde{t}_1}$ and on m_{min}, which is the lightest other SUSY particle in the loop except for $m_{\tilde{t}_2}$, i. e. $m_{min} = \text{Min}\{\text{m}_{\tilde{\text{g}}}, \text{m}_{\tilde{\chi}_{1,2,3,4}}, \text{m}_{\tilde{\text{u}}_{1,2}}, \text{m}_{\tilde{\text{d}}_{1,2}}\}$. For small masses of $m_{\tilde{t}_1} < 200$ GeV and $m_{min} < 200$ GeV, the upper bound on $A_{\rm FB}^{t\bar{t}}$ is with up to $+3\%$ somewhat larger than the absolute value of the lower bound with -2%. This is because the SUSY QCD bounds, Eq. (24), are in general not symmetric and in this region the contribution from $A_{q,ij}^{(3)}$ is non-negligible and positive as shown in Fig. 4.

In general, one observes that smaller up-squark masses $m_{\tilde{u}_1}$ and top squark masses $m_{\tilde{t}_1}$ lead to larger MSSM one-loop contributions to the forward-backward asymmetry. The same is valid for the gluino mass when $m_{\tilde{g}} > 250$ GeV. For $m_{\tilde{g}} < 250$ GeV the asymmetry is dominated by the contribution of the resonant gluino pair. Since the SUSY EW one-loop corrections are sub-leading, the asymmetry has a very small dependence on the neutralino mass. Furthermore, the asymmetry is larger for a larger mass splitting of $m_{\tilde{t}_1}$ and $m_{\tilde{t}_2}$. This is illustrated for the lower bound on $A_{\rm FB}^{t\bar{t}}$ in Fig. 9(a) and the upper bound on $A_{\rm FB}^{t\bar{t}}$ in Fig. 9(b), where $A_{min,max}$ are shown in dependence of $m_{\tilde{t}_2} - m_{\tilde{t}_1}$ and on m_{min}, which here is the lightest SUSY particle in the loops, i. e. $m_{min} = \text{Min}\{\text{m}_{\tilde{\text{t}}_{1,2}}, \text{m}_{\tilde{\text{g}}}, \text{m}_{\tilde{\chi}_{1,2,3,4}}, \text{m}_{\tilde{\text{u}}_{1,2}}, \text{m}_{\tilde{\text{d}}_{1,2}}\}$.

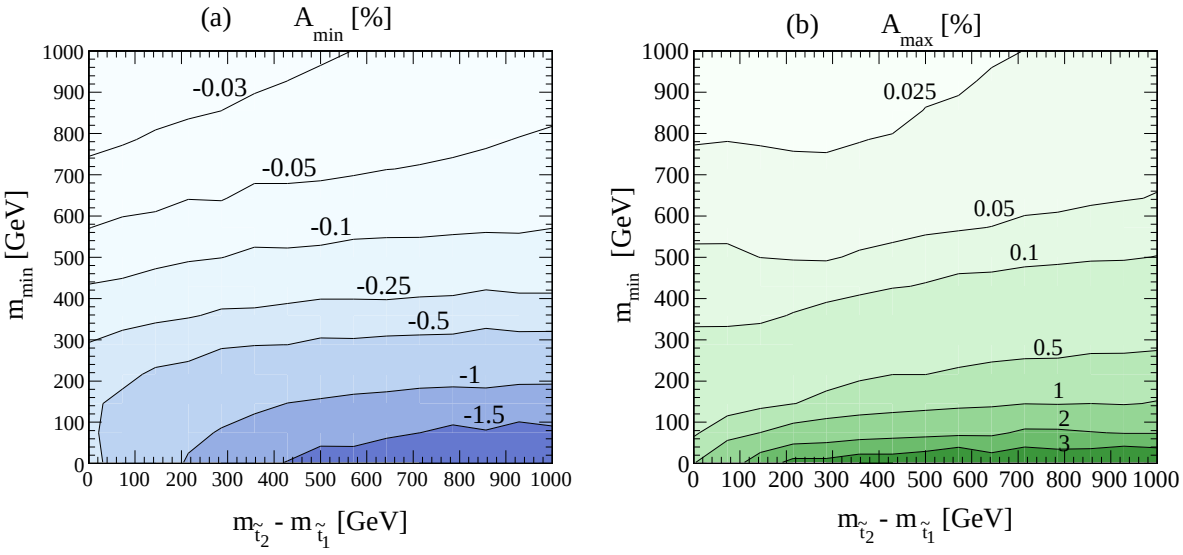

Figure 9: Bounds on the MSSM one-loop contributions to $A_{\rm FB}^{t\bar{t}}$ with $M_{t\bar{t}} > 450$ GeV: (a) Lower and (b) upper bounds on $A_{\rm FB}^{t\bar{t}}$ (in percent) as functions of the stop mass splitting $m_{\tilde{t}_2} - m_{\tilde{t}_1}$ and m_{min}, which is the lightest SUSY particle in the loops, i. e. $m_{min} = \text{Min}\{\text{m}_{\tilde{\text{t}}_{1,2}}, \text{m}_{\tilde{\text{g}}}, \text{m}_{\tilde{\chi}_{1,2,3,4}}, \text{m}_{\tilde{\text{u}}_{1,2}}, \text{m}_{\tilde{\text{d}}_{1,2}}\}$.

As can be seen, when the stop masses are degenerate, then even for tiny m_{min} one finds $-0.5\% < A_{\rm FB}^{t\bar{t}} < +1\%$. For a stop mass splitting of $m_{\tilde{t}_2} - m_{\tilde{t}_1} = 500$ GeV and $m_{min} > 300$ GeV one can obtain bounds up to $|A_{min,max}| = 0.5\%$. Larger values for the asymmetry are possible when the stop mass splitting is even larger and $m_{min} < 300$ GeV. A similar behavior, but not as pronounced, can be observed for the up-squark mass splitting $m_{\tilde{u}_2} - m_{\tilde{u}_1}$. For the bounds shown in Fig. 9(a) and Fig. 9(b), $\tilde{u}_2$ is basically decoupled and $m_{\tilde{u}_1} \approx m_{min}$. In the case when the two up-squark mass eigenstates are degenerate and $m_{\tilde{u}} \approx m_{min} > 100$ GeV, one can roughly divide the given limits of Fig. 9 by a factor of two to obtain the limits for the case of degenerate up-squark masses $m_{\tilde{u}_1} = m_{\tilde{u}_2}$. For $m_{\tilde{u}} \approx m_{min} < 100$ GeV the limits decrease only mildly.

As discussed earlier, SUSY searches at the LHC, interpreted in the CMSSM and Simplified Models, impose stringent limits on the masses of squarks and gluinos. An updated summary of the limits obtained by CMS and ATLAS can be found in Refs. [58, 59]. In the following we illustrate the impact of some of these limits on the bounds on $A_{\rm FB}^{t\bar{t}}$. For instance, ATLAS SUSY searches in events with jets and missing transverse energy interpreted in the CMSSM find that gluinos and squarks lighter than about 950 GeV [48, 59] are ruled out for $m_{\tilde{g}} = m_{\tilde{q}}$, while for $m_{\tilde{q}} \gg m_{\tilde{g}}$ the gluino can be somewhat lighter, i. e. $m_{\tilde{g}} > 680$ GeV [59, 60] for $m_{\tilde{q}} = 2m_{\tilde{g}}$ (all limits are at 95% C. L.). Note that these squark mass limits do not apply for the third generation squarks due to slightly different production mechanisms for stops and sbottoms and the different decay pattern of top squarks. As can be seen in Fig. 8, in this scenario with $m_{\tilde{g}} = m_{min} = 680$ GeV the upper bound on $A_{\rm FB}^{t\bar{t}}$ can be at most $A_{max} \approx 0.15\%$ for $m_{\tilde{t}_1} \lesssim 200$ GeV.

Note that these mass limits depend on the assumptions that go into the extraction of the limits. For instance, when $m_{\tilde{g}} \gg m_{\tilde{q}}$ the SUSY signal is dominated by squark pair production in the $gg \to \tilde{q}\bar{\tilde{q}}$ channel and thus is proportional to the number of degenerate squarks. The signal cross section drops significantly if all but one squark are decoupled, which weakens the mass limits obtained under assumptions of degenerate squarks. The sensitivity of these SUSY searches also drops when the neutralino mass $m_{\tilde{\chi}_1^0}$ is increased. For example, as shown in Ref. [58] the CMS limit on the gluino mass obtained in a Simplified Model decreases from about 850 GeV to 400 GeV, if the neutralino mass is increased from 0 GeV to $m_{\tilde{g}} - 200$ GeV. In this scenario, the upper bound on $A_{\rm FB}^{t\bar{t}}$ increases from about 0.1% ($m_{min} = 850$ GeV) to $A_{max} \approx 0.5\%$ ($m_{min} = 400$ GeV) for $m_{\tilde{t}_1} \lesssim 200$ GeV, as shown in Fig. 8.
Moreover, the extraction of mass limits on squarks and gluinos gets even more involved if the (light) squarks do not decay directly into the lightest neutralino. And finally, one might consider MSSM scenarios where the neutralino is not the LSP. The LHC SUSY searches of Refs. [45, 48, 61] do not strictly require a neutralino LSP. They remain valid as long as squarks and gluinos decay dominantly into missing energy and one or two jets, respectively. A different type of analysis is required if colored SUSY particles are stable or quasi-stable. This can, for example, happen in gauge mediated SUSY breaking scenarios with a gravitino LSP and a squark next-to-LSP (NLSP). Stable or quasi-stable SUSY particles would form so-called *R*-hadrons with specific detector signals. A search for *R*-hadrons was presented in Ref. [62] and mass limits of 300 GeV and 600 GeV are given for (quasi-)stable squarks and gluinos, respectively. Again with smaller squark/gluino mass, the bounds on $A_{\rm FB}^{t\bar{t}}$ increase in this scenario from about 0.25% ($m_{min} = 600$ GeV) to almost $|A_{min,max}| \approx 1\%$ ($m_{min} = 300$ GeV) for $m_{\tilde{t}_1} \lesssim 100$ GeV, as shown in Fig. 8.
As illustrated on these examples, since our results for the bounds on the forward-backward asymmetry have been obtained with the only assumption that we work within the MFV-MSSM, the impact of a number of specific scenarios on the upper and lower bounds on $A_{\rm FB}^{t\bar{t}}$ can be estimated.

IV. CONCLUSIONS

The study of asymmetries in $t\bar{t}$ production, such as the forward-backward charge asymmetry, parity violating asymmetries in polarized $t\bar{t}$ production, and spin correlations between the t and $\bar{t}$, may provide a window to non-SM physics complementary to direct searches for non-SM particles. A recent measurement of the corrected (parton-level) forward-backward charge asymmetry in $t\bar{t}$ production at the Tevatron deviates from the SM prediction by about 3σ in the region $M_{t\bar{t}} > 450$ GeV. Provided the SM prediction is under good theoretical control, this discrepancy may leave room for an interpretation as a signal of non-SM physics, and a number of non-SM scenarios have been proposed in the literature. In this paper we calculated the SUSY EW and SUSY QCD one-loop corrections to $A_{\rm FB}^{t\bar{t}}$ within the MFV-MSSM

and derived general lower and upper bounds A_{min}, A_{max} on $A_{\rm FB}^{t\bar{t}}$ at the Tevatron by performing a comprehensive scan over the relevant MSSM parameter space. Since the MSSM one-loop corrections to $A_{\rm FB}^{t\bar{t}}$ are dominated by SUSY QCD one-loop corrections, these bounds strongly depend on the squark and gluino masses and are much less affected by the neutralino mass. As expected, these loop effects are more pronounced for smaller sparticle masses in the loops and larger stop/squark mass splittings. For very small masses, $m_{\tilde{t}_1} < 200$ GeV and $m_{min} = \text{Min}\{\text{m}_{\tilde{\text{g}}}, \text{m}_{\tilde{\text{u}}_{1,2}}, \text{m}_{\tilde{\text{d}}_{1,2}}\} < 200$ GeV, we find $-2\% < A_{\rm FB}^{t\bar{t}} < +3\%$, which is comparable in size to the SM EW corrections to $A_{\rm FB}^{t\bar{t}}$. This is the maximum possible SUSY loop-induced asymmetry that can be obtained within the MFV-MSSM at the Tevatron, with $M_{t\bar{t}} > 450$ GeV. It is important to emphasize that apart from working within the MFV-MSSM, no additional assumptions or constraints have been imposed in our derivation of the bounds on $A_{\rm FB}^{t\bar{t}}$ and that from the general bounds presented in this paper an estimate can be obtained of how they change when assuming a specific SUSY scenario. For example, to illustrate the impact of squark and gluino mass limits obtained within the CMSSM at the LHC, we obtain from the results presented in Fig. 8 that for gluino and squark masses in the range 850 GeV-1000 GeV, $A_{max} \approx 0.1\%$ for a light top squark of $m_{\tilde{t}_1} = 200$ GeV and $m_{min} = 850$ GeV, and $A_{max} \approx 0.05\%$ for $m_{\tilde{t}_1} = 600$ GeV and $m_{min} = 1$ TeV.

Acknowledgments

The work of S. B. is supported by the Initiative and Networking Fund of the Helmholtz Association, contract HA-101 ('Physics at the Terascale') and by the Research Center 'Elementary Forces and Mathematical Foundations' of the Johannes-Gutenberg-Universität Mainz. The work of D. W. is supported by the National Science Foundation under grant No. NSF-PHY-0547564 and No. NSF-PHY-0757691. The work of M. W. is partially supported by project DFG NI 1105/2-1.

V. APPENDIX

A. Gluino-squark-quark couplings

The gluino-squark-quark couplings as defined in Eq. (7) are [39]

$$g_n^{\pm} = i\sqrt{2} g_s \hat{g}_n^{\pm} \quad \text{with} \tag{28}$$

$$\hat{g}_1^{\lambda} = \lambda U_{i,\lambda}^{\tilde{q}} e^{i\lambda\phi/2} \quad , \quad \hat{g}_4^{\lambda} = \lambda U_{j,\lambda}^{\tilde{t}} e^{i\lambda\phi/2} \quad , \quad (\lambda = +,-)\,. \tag{29}$$

The index i and j have been omitted in the definition of $g_n^{\pm}$ of Eq. (28) to avoid large chains of indices in Section II. The index i always refers to the squark index of flavor $q = \{u, d, s, c, b\}$ of the vertices Γ_1 and Γ_2 and the index j always refers to the stop quark index of Γ_3 and Γ_4.

The complex phase of the gluino mass M_3 is denoted by ϕ. The couplings are related by

$$\hat{g}_2^{\pm} = \hat{g}_1^{\mp *} \quad , \qquad \hat{g}_3^{\pm} = \hat{g}_4^{\mp *}.$$

The unitary squark mixing matrices are given as

$$U^{\tilde{q}} = \begin{pmatrix} U_{1,-}^{\tilde{q}} & U_{1,+}^{\tilde{q}} \\ U_{2,-}^{\tilde{q}} & U_{2,+}^{\tilde{q}} \end{pmatrix} \quad , \qquad U^{\tilde{t}} = \begin{pmatrix} U_{1,-}^{\tilde{t}} & U_{1,+}^{\tilde{t}} \\ U_{2,-}^{\tilde{t}} & U_{2,+}^{\tilde{t}} \end{pmatrix} \tag{30}$$

For the squark mass and mixing matrices we use the conventions of Ref. [39].

B. Neutralino-squark-quark couplings

For the neutralino-squark-quark couplings, we again follow the notation of Ref. [39] , where explicit expressions for these couplings can be found. For completeness, since the $u\bar{u}$-channel is the dominant $t\bar{t}$ production process, we provide here the neutralino-up-quark-squark coupling, which reads with the restriction $m_u = 0$ GeV [39]:

$$\begin{aligned} g_n^{\pm} &= i\sqrt{2}e\hat{g}_n^{\pm} \qquad \text{with} \qquad (31) \\ \hat{g}_1^{+} &= \frac{2}{3c_W} \cdot N_{k,1} \cdot U_{i,+}^{\tilde{u}} \\ \hat{g}_1^{-} &= -\frac{1}{2s_W} \cdot N_{k,2}^{*} \cdot U_{i,-}^{\tilde{u}} - \frac{1}{6c_W} \cdot N_{k,1}^{*} \cdot U_{i,-}^{\tilde{u}} \\ \hat{g}_4^{+} &= \frac{1}{6c_W s_W m_W s_\beta} \cdot \left[4m_W s_\beta s_W N_{k,1} \cdot U_{j,+}^{\tilde{t}} - 3c_W m_t N_{k,4} \cdot U_{j,-}^{\tilde{t}} \right] \\ \hat{g}_4^{-} &= \frac{-1}{6c_W s_W m_W s_\beta} \cdot \left[\left(3c_W m_W s_\beta N_{k,2}^{*} + s_W m_W s_\beta N_{k,1}^{*} \right) \cdot U_{j,-}^{\tilde{t}} + 3c_W m_t N_{k,4}^{*} \cdot U_{j,+}^{\tilde{t}} \right] \qquad (32) \end{aligned}$$

where we used the shorthand notations $c_W = \cos\theta_W, s_W = \sin\theta_W$ and $s_\beta = \sin\beta$ with $\tan\beta = \frac{v_u}{v_d}$ the ratio of the two Higgs field vacuum expectation values. Here the coupling parameters are related by

$$g_2^{\pm} = g_1^{\mp *} \quad , \qquad g_3^{\pm} = g_4^{\mp *}.$$

The neutralino mass matrices in the used convention have been taken from Ref. [63].

C. Analytic Expressions for the one-loop functions D^a

The partonic differential cross section $\frac{d\hat{\sigma}^{(a,b)}}{d\cos\theta}$ for the direct box diagrams of Fig. 1(a) and crossed box of Fig. 1(b) are given in Eq. (8) and Eq. (10), respectively, in terms of coupling parameters and loop functions D^a. Neglecting the initial-state quark masses and using the mass assignments of Fig. 1, the functions $D^a(\hat{s}, \cos\theta)$ are given with $\hat{t} = m_t^2 - \frac{\hat{s}}{2}(1 - \beta_t \cos\theta)$

as

$$
\begin{aligned}
D^{+-++}(\hat{s},\cos\theta) &= -\frac{1}{32\pi^2\hat{s}}\cdot\left[-m_2 m_t \hat{s}^2 D_1 + \left(-m_t^4 - m_t^2\hat{s} + 2m_t^2\hat{t} - \hat{t}^2\right) m_t m_2 D_2\right] \\
D^{-+++}(\hat{s},\cos\theta) &= -\frac{1}{32\pi^2\hat{s}}\cdot m_t m_4\left[\left(-m_t^4 - m_t^2\hat{s} + 2m_t^2\hat{t} - \hat{t}^2\right) D_2 - \hat{s}^2 D_3\right] \\
D^{-++-}(\hat{s},\cos\theta) &= -\frac{1}{32\pi^2\hat{s}}\cdot\left\{D_{00}\cdot\left(-2m_t^4 + 2m_t^2\hat{s} + 4m_t^2\hat{t} - 2\hat{s}^2 - 4\hat{s}\hat{t} - 2\hat{t}^2\right)\right. \\
&\qquad + m_t^2\hat{s}^2 D_{12} + \left(m_t^4\hat{s} - m_t^2\hat{s}^2 - 2m_t^2\hat{s}\hat{t} + \hat{s}^3 + 2\hat{s}^2\hat{t} + \hat{s}\hat{t}^2\right) D_{13} \\
&\qquad \left. + \left(m_t^6 + m_t^4\hat{s} - 2m_t^4\hat{t} + m_t^2\cdot\hat{t}^2\right) D_{22} + m_t^2\hat{s}^2 D_{23}\right\} \\
D^{-+-+}(\hat{s},\cos\theta) &= -\frac{1}{32\pi^2\hat{s}}\cdot m_2 m_4\cdot\left(m_t^4 + m_t^2\hat{s} - 2m_t^2\hat{t} + \hat{t}^2\right) D_0, \qquad (33)
\end{aligned}
$$

where $D_{i,ij} = D_{i,ij}\left(0, m_t^2, m_t^2, 0, \hat{t}, \hat{s}, m_1^2, m_2^2, m_3^2, m_4^2\right)$ are written in the convention of Ref. [43]. From these expressions the contribution to Fig. 1(b) can be obtained by replacing $D^a(\hat{s},\cos\theta) \to D^a(\hat{s},-\cos\theta)$ and multiplying by a factor of (-1) for exchanging the final-state fermions.

---

[1] Aaltonen, T. and others, *Phys.Rev.Lett.* 101 (2008) 202001 [0806.2472].

[2] Aaltonen, T. and others, *Phys.Rev.* D83 (2011) 112003 [1101.0034].

[3] The CDF Collaboration. (2011) [CDF Conf. Note 10584].

[4] Abazov, V.M. and others, *Phys.Rev.Lett.* 100 (2008) 142002 [0712.0851].

[5] Abazov, Victor Mukhamedovich and others, *Phys. Rev.* D84 (2011) 112005 [1107.4995].

[6] Kühn, Johann H. and Rodrigo, German, *Phys. Rev.* D59 (1999) 054017 [hep-ph/9807420].

[7] Kühn, Johann H. and Rodrigo, German, *Phys. Rev. Lett.* 81 (1998) 49–52 [hep-ph/9802268].

[8] Bowen, M. T. and Ellis, S. D. and Rainwater, D., *Phys. Rev.* D73 (2006) 014008 [hep-ph/0509267].

[9] Antunano, Oscar and Kühn, Johann H. and Rodrigo, German, *Phys. Rev.* D77 (2008) 014003 [0709.1652].

[10] Almeida, Leandro G. and Sterman, George F. and Vogelsang, Werner, *Phys. Rev.* D78 (2008) 014008 [0805.1885].

[11] Ahrens, Valentin and Ferroglia, Andrea and Neubert, Matthias and Pecjak, Ben D. and Yang, Li Lin, *Phys. Rev.* D84 (2011) 074004 [1106.6051].

[12] Hollik, Wolfgang and Pagani, Davide, *Phys. Rev.* D84 (2011) 093003 [1107.2606].

[13] Kühn, Johann H. and Rodrigo, German, *JHEP*. 01 (2012) 063 [1109.6830].

[14] Manohar, Aneesh V. and Trott, Michael. (2012) [1201.3926].

[15] Kidonakis, Nikolaos, *Phys. Rev.* D84 (2011) 011504 [1105.5167].

[16] Aguilar-Saavedra, J. A. and Perez-Victoria, M., *JHEP.* 1109 (2011) 097 [1107.0841].

[17] Davoudiasl, Hooman and McElmurry, Thomas and Soni, Amarjit. (2011) [1108.1173].

[18] Cui, Yanou and Han, Zhenyu and Schwartz, Matthew D., *JHEP*. 07 (2011) 127 [1106.3086].

[19] Isidori, Gino and Kamenik, Jernej F., *Phys. Lett.* B700 (2011) 145–149 [1103.0016].

[20] Nilles, Hans Peter, *Phys. Rept.* 110 (1984) 1.

[21] Haber, Howard E. and Kane, Gordon L., *Phys. Rept.* 117 (1985) 75.

[22] Buras, A.J. and Gambino, P. and Gorbahn, M. and Jager, S. and Silvestrini, L., *Phys.Lett.* B500 (2001) 161–167 [hep-ph/0007085].

[23] D'Ambrosio, G. and Giudice, G.F. and Isidori, G. and Strumia, A., *Nucl.Phys.* B645 (2002) 155–187 [hep-ph/0207036].

[24] Li, Chong-Sheng and Hu, Bing-Quan and Yang, Jin-Min and Hu, Chen-Guo, *Phys. Rev.* D52 (1995) 5014–5017.

[25] Alam, S. and Hagiwara, K. and Matsumoto, S., *Phys. Rev.* D55 (1997) 1307–1315 [hep-ph/9607466].

[26] Sullivan, Zack, *Phys. Rev.* D56 (1997) 451–457 [hep-ph/9611302].

[27] Zhou, Hong-Yi and Li, Chong-Sheng, *Phys. Rev.* D55 (1997) 4421–4429.

[28] Yu, Zeng-Hui and Pietschmann, H. and Ma, Wen-Gan and Han, Liang and Yi, Jiang, *Eur. Phys. J.* C9 (1999) 463–477 [hep-ph/9804331].

[29] Wackeroth, D. (1998) [hep-ph/9807558].

[30] Berge, Stefan and Hollik, Wolfgang and Mosle, Wolf M. and Wackeroth, Doreen, *Phys. Rev.* D76 (2007) 034016 [hep-ph/0703016].

[31] Ross, D. A. and Wiebusch, M., *JHEP*. 11 (2007) 041 [0707.4402].

[32] Yang, Jin-Min and Li, Chong-Sheng, *Phys. Rev.* D52 (1995) 1541–1545.

[33] Yang, Jin Min and Li, Chong Sheng, *Phys. Rev.* D54 (1996) 4380–4384 [hep-ph/9603442].

[34] Kim, Jaewan and Lopez, Jorge L. and Nanopoulos, D. V. and Rangarajan, R., *Phys. Rev.* D54 (1996) 4364–4373 [hep-ph/9605419].

[35] Hollik, W. and Mosle, W. M. and Wackeroth, D., *Nucl. Phys.* B516 (1998) 29–54 [hep-ph/9706218].

[36] Denner, A. and Eck, H. and Hahn, O. and Küblbeck, J., *Nucl. Phys.* B387 (1992) 467–484.

[37] Küblbeck, J. and Böhm, M. and Denner, A., *Comput. Phys. Commun.* 60 (1990) 165–180.

[38] Hahn, Thomas, *Comput. Phys. Commun.* 140 (2001) 418–431 [hep-ph/0012260].

[39] Hahn, Thomas and Schappacher, Christian, *Comput. Phys. Commun.* 143 (2002) 54–68 [hep-ph/0105349].

[40] Passarino, G. and Veltman, M. J. G., *Nucl. Phys.* B160 (1979) 151.

[41] Vermaseren, J.A.M. (2000) [math-ph/0010025].

[42] Pumplin, J. and others, *JHEP*. 07 (2002) 012 [hep-ph/0201195].

[43] Hahn, T. and Perez-Victoria, M., *Comput.Phys.Commun.* 118 (1999) 153–165 [hep-ph/9807565].

[44] Nakamura, K. and others, *J. Phys.* G37 (2010) 075021.

[45] Chatrchyan, Serguei and others, *Phys. Rev. Lett.* 107 (2011) 221804 [1109.2352].

[46] Chatrchyan, Serguei and others, *Phys. Rev.* D85 (2012) 012004 [1107.1279].

[47] Khachatryan, Vardan and others, *Phys. Lett.* B698 (2011) 196–218 [1101.1628].

[48] Aad, Georges and others. (2011) [1109.6572].

[49] Aad, Georges and others, *Phys. Rev.* D85 (2012) 012006 [1109.6606].

[50] Aad, Georges and others, *Phys. Rev. Lett.* 106 (2011) 131802 [1102.2357].

[51] da Costa, Joao Barreiro Guimaraes and others, *Phys. Lett.* B701 (2011) 186–203 [1102.5290].

[52] Landau, L. D., *Nucl. Phys.* 13 (1959) 181–192.

[53] Djouadi, Abdelhak and Kneur, Jean-Loic and Moultaka, Gilbert, *Comput.Phys.Commun.* 176 (2007) 426–455 [hep-ph/0211331].

[54] `http://hepsource.sf.net/dvegas`.

[55] Kauer, N. and Zeppenfeld, D., *Phys.Rev.* D65 (2002) 014021 [hep-ph/0107181].

[56] Kauer, N., *Phys.Rev.* D67 (2003) 054013 [hep-ph/0212091].

[57] Brein, Oliver, *Comput. Phys. Commun.* 170 (2005) 42–48 [hep-ph/0407340].

[58] Koay, S.A. and Collaboration, CMS. (2012) [1202.1000].

[59] M Fehling-Kaschek. Supersymmetry searches at atlas. Technical Report ATL-PHYS-PROC-2012-039, CERN, Geneva, Feb 2012.

[60] Aad, Georges and others, *JHEP*. 11 (2011) 099 [1110.2299].

[61] Search for supersymmetry in pp 1 collisions at sqrt(s) = 7 tev in final states with missing transverse momentum, b-jets and one lepton with the atlas detector. Technical Report ATLAS-CONF-2011-130, CERN, Geneva, Sep 2011.

[62] Aad, Georges and others, *Phys.Lett.* B701 (2011) 1–19 [1103.1984].

[63] Frank, M. and Hahn, T. and Heinemeyer, S. and Hollik, W. and Rzehak, H. and others, *JHEP*. 0702 (2007) 047 [hep-ph/0611326].